

Article

Structural and Optical Characterization of a New Tetra- and Hexa-Coordinated Cd-Based Hybrid Compound with White Light Emission

Imen Sayer¹, Rawia Msalmi¹, Edoardo Mosconi², Ahlem Guesmi³ , Ammar Houas⁴, Naoufel Ben Hamadi³ 
and Houcine Naili^{1,*} 

- ¹ Laboratory Physico Chemistry of the Solid State, Department of Chemistry, Faculty of Sciences of Sfax, Sfax University, Sfax 3000, Tunisia; imen.sayer@fss.rnu.tn (I.S.); rawia.msalmi@fss.rnu.tn (R.M.)
- ² Computational Laboratory for Hybrid/Organic Photovoltaics (CLHYO), Istituto CNR di Scienze e Tecnologie Chimiche “Giulio Natta” (CNR-SCITEC), Via Elce di Sotto 8, 06123 Perugia, Italy; edoardo@thch.unipg.it
- ³ Chemistry Department, College of Science, Imam Mohammad Ibn Saud Islamic University (IMSIU), P.O. Box 5701, Riyadh 11432, Saudi Arabia; amalkasme@imamu.edu.sa (A.G.); nabenhamadi@imamu.edu.sa (N.B.H.)
- ⁴ Research Laboratory of Catalysis and Materials for Environment and Processes, University of Gabes, City Riadh Zerig, Gabes 6029, Tunisia; amahouas@univgb.tn
- * Correspondence: houcine.naili@fss.rnu.tn

Abstract: The present paper deals with a new two-in-one zero-dimensional (0D) organic–inorganic hybrid compound namely $(C_6H_{10}N_2)_4[CdBr_6][CdBr_4]_2$. This molecular crystal structure contains isolated $CdBr_4$ tetrahedra and $CdBr_6$ octahedra. The optical characterization by UV–Vis–NIR spectroscopy shows that the $(C_6H_{10}N_2)_4[CdBr_6][CdBr_4]_2$ exhibits a large gap energy of 4.97 eV. Under UV excitation, this hybrid material shows a bright cold white light emission (WLE) at room temperature. The photoluminescence (PL) analysis suggests that the WLE originates from the organic molecules. Density of states (DOS) analysis using the density functional theory (DFT) demonstrates that the calculated HOMO(Br)→LUMO(organic) absorption transition (4.1 eV) does not have significant intensity, while, the transition involving the valence band (VB) and the second and third conduction bands (CB) around 5 eV are allowed, which is in good agreement with the experimental gap value. The interesting theoretical result is that the LUMO(organic)→HOMO(Br) emission is allowed, which confirms the important role of the organic molecule in the emission mechanism, in good agreement with the experimental PL analysis.

Keywords: Cd-based hybrid; optical absorption; band gap; white light emission; DFT calculations



Citation: Sayer, I.; Msalmi, R.; Mosconi, E.; Guesmi, A.; Houas, A.; Ben Hamadi, N.; Naili, H. Structural and Optical Characterization of a New Tetra- and Hexa-Coordinated Cd-Based Hybrid Compound with White Light Emission. *Crystals* **2024**, *14*, 459. <https://doi.org/10.3390/cryst14050459>

Academic Editor: Ioannis Spanopoulos

Received: 18 March 2024
Revised: 19 April 2024
Accepted: 10 May 2024
Published: 12 May 2024



Copyright: © 2024 by the authors. Licensee MDPI, Basel, Switzerland. This article is an open access article distributed under the terms and conditions of the Creative Commons Attribution (CC BY) license (<https://creativecommons.org/licenses/by/4.0/>).

1. Introduction

Organic–inorganic hybrid compounds have evoked great attention as some of the most promising materials in the application of solid-state lighting [1–9], light-emitting diodes [10–16], and optical sensors [17,18]. Up to now, achieving white light emission has been recognized as a critical step for solid-state lighting to become a more efficient lighting source than conventional ones [19–23]. Very recently, low-dimensional Cd-based organic–inorganic semiconductors, with tetrahedral or octahedral coordination around the Cd cations, proved their fascinating luminescent properties as solid state white light emitters [24–31]. Scrutiny of the luminescence response of the previously studied Cd-based hybrid materials revealed that their emission behavior is very similar to that observed for pure CdX_2 ($X = Cl, Br$ and I) [32–34]. The emission bands of the pure CdX_2 compounds, observed in the range of 326–620 nm, are assigned to the self-trapped excitons (STE). These STE generate a broad emission spanning the majority of the visible spectrum giving rise to white photoluminescence. For example, in the 2D perovskite $(CH_3NH_3)_2CdCl_4$ reported by R. Rocanova et al., the broadband white light emission (WLE) is attributed

to the formation of STE in the CdCl_6 octahedra [33]. In this context, the selection of the excitation wavelengths should be carried out with reference to the band gap energy value. In fact, the improvement in the self-trapping mechanism of excitons within the octahedral and the tetrahedral inorganic polyhedra of organic–inorganic hybrid materials needs a sub-gap excitation ($E_{\text{Exc}} < E_g$). In $(\text{C}_6(\text{CH}_3)_5\text{CH}_2\text{N}(\text{CH}_3)_3) \text{CdBr}_4 \cdot \text{DMSO}$, the white light emission was assigned to the STE within CdBr_4 tetrahedra [34], while the emission observed from the $(\text{Ph}_4\text{P})_2\text{CdBr}_4$ was assigned to the high fluorescence and the weak RTP of the organic moieties [35]. Recently, R. Msalmi et al. reported the photoluminescence behavior of two zero-dimensional Cd-based hybrid compounds where the white light emission was observed using both sub-gap excitation energy and upper the gap excitation energy [29]. The authors indicated that the emission under excitation energy above the gap value results from the fluorescence and/or phosphorescence of π -conjugated aromatic cations, while the broad emission under sub-gap excitation is a combination of organic fluorescence and/or phosphorescence and the white emission from STE inside the inorganic anions [29]. In this work, we present a new organic–inorganic Cd-based hybrid compound $(\text{C}_6\text{H}_{10}\text{N}_2)_4[\text{CdBr}_6][\text{CdBr}_4]_2$, containing tetra- and octahedral Cd^{2+} anions ($[\text{CdBr}_4]^{2-}$ and $[\text{CdBr}_6]^{4-}$). To our knowledge, “two-in-one” hybrid Cd-based complexes with two different coordination around the Cd(II) centers, are rare and still need to be inspected for their relevant optical and photoluminescent behavior [30,36]. The crystal structure of the synthesized compound is determined by X-ray diffraction and analyzed with FTIR spectroscopy. The thermal stability is examined up to 1000 °C. The optical behaviors are also studied using UV–Vis–NIR absorption and photoluminescence spectroscopy.

2. Experimental Analysis

2.1. Synthesis Method

For the preparation of the target compound, the following commercially available starting reagents were used without purification: $\text{C}_6\text{H}_8\text{N}_2$ (2-picolyamine) (97%), cadmium bromide dihydrate ($\text{CdBr}_2 \cdot 2\text{H}_2\text{O}$) (98%) and hydrobromic acid (HBr) (48%). First, 0.103 mL (1 mmol) of the $\text{C}_6\text{H}_8\text{N}_2$ was added to 10 mL of heated aqueous solution, containing 0.344 g (1 mmol) of $\text{CdBr}_2 \cdot 4\text{H}_2\text{O}$ and 1 mL of hydrobromic acid HBr (48%). The resultant solution was stirred for 30 min until complete dissolution and allowed to stand at room temperature. After a few days, white crystals appeared.

2.2. Structure Determination

Crystal diffraction intensities of a suitable single crystal with size of $0.10 \times 0.03 \times 0.03 \text{ mm}^3$ were collected at room temperature using an APEXII, Bruker-AXS diffractometer (Bruker-AXS, Karlsruhe (or State), Germany) using $\lambda(\text{MoK}\alpha) = 0.71073 \text{ \AA}$. The various structural parameters were refined by the least-squares method applied to the square of the structural factors modules $|F_2|$, using SHELXS/SHELXL 2018 [37]. The material was found to crystallize in the triclinic symmetry $\text{P}\bar{1}$ space group. Atomic positions and thermal factors were calculated following a series of refinements. Meanwhile, all the hydrogen atoms of the phenyl groups were geometrically fixed. The refinement converged with final discrepancy factors: $R_1 = 0.0297$, $wR_2 = 0.0591$ and $\text{GooF} = 0.991$ for $(\text{C}_6\text{H}_{10}\text{N}_2)_4[\text{CdBr}_6][\text{CdBr}_4]_2$. Table 1 lists all of the recording data of intensities and structure resolution (CCDC-2278443, Supplementary Materials).

The elemental analysis was performed to confirm the composition of the sample to be H: 2.097 (3)% (theor. 2.125%), N: 6.002 (3)% (theor. 5.908%) and C: 15.436 (3)% (theor. 15.419%). The analysis of the halogens shows that the Br atoms present 59.264 (5)% (theor. 59.274%) of the total weight of the sample. The obtained experimental values confirm the molecular formula of the compound and its phase purity.

Table 1. Crystal data and refinement parameters of $(C_6H_{10}N_2)_4[CdBr_6][CdBr_4]_2$.

Empirical formula	$(C_6H_{10}N_2)_4[CdBr_6][CdBr_4]_2$
Formula weight (g. mol ⁻¹)	1896.47
Temperature (K)	296 (2)
Crystal system	Triclinic
Space group	$P\bar{1}$
a (Å)	7.9551 (3)
b (Å)	12.7497 (6)
c (Å)	13.5271 (6)
α (°)	65.249 (2)
β (°)	80.351 (2)
γ (°)	75.455 (2)
V (Å ³)	1202.97 (9)
Z	1
Crystal size (mm ³)	0.10 × 0.03 × 0.03
Color	Brown
λ (MoK α) (Å)	0.71073
Absorption correction	Multi- scan
No. of collected reflections	46856
No. of independent reflections	4229
No. of observed reflections ($I > 2\sigma(I)$)	3213
No. of parameters	223
T_{min}	0.357
T_{max}	0.697
Index range	$-9 \leq h \leq 9$ $-15 \leq k \leq 15$ $-16 \leq l \leq 16$
R1	0.0297
wR2	0.0591
Goof	0.991

2.3. Physico-Chemical Characterizations

The thermal decomposition of $(C_6H_{10}N_2)_4[CdBr_6][CdBr_4]_2$ was studied by TGA analysis under nitrogen flow. The thermogram was collected in a temperature range of 30 to 1000 °C with a heating rate of 10 °C/min. The infrared spectrum was recorded in the 500–4000 cm⁻¹ range using a Perkin Elmer 1600 FT-IR Spectrometer (Perkin Elmer, Massachusetts, United States). The diffuse reflectance spectrum was measured using a UV–Vis–NIR spectrophotometer at room temperature in the wavelength range {200–1100 nm}. The UV–Vis diffuse reflectance spectrum of the synthesized compound was recorded at room temperature using a Varian Cary 5000 UV–Vis–NIR spectrophotometer (Varian, California, United States). The PL spectra were collected using a Horiba FluoroMax 4 spectrometer (Horiba Scientific, Kyoto, Japan) at room temperature under different excitation wavelengths.

3. Results and Discussion

3.1. Crystal Structure

$(C_6H_{10}N_2)_4[CdBr_6][CdBr_4]_2$ crystallizes in the triclinic space group $P\bar{1}$ with the cell parameters indicated in Table 1. The asymmetric unit of $(C_6H_{10}N_2)_4[CdBr_6][CdBr_4]_2$ consists of two deprotonated 2-ammoniummethylpyridinium cations $[C_6H_{10}N_2]^{2+}$, one tetrahedral $[CdBr_4]^{2-}$ anion and one anionic fragment $[CdBr_3]^-$ (Figure 1a). The visualization of the coordination sphere around the Cd cations shows that Cd1 is hexacoordinated to six Br ions, which are completed by symmetry, to adopt an octahedral geometry (Figure 1b). The coexistence of both tetrahedral and octahedral coordination around the Cd(II) ions is a spell-binding structural aspect of this complex. This compound is similar to $[C_5H_9-NH_3]_4CdBr_6$ where four- and hexa-coordinated Cd(II) ions are observed within the structure [30].

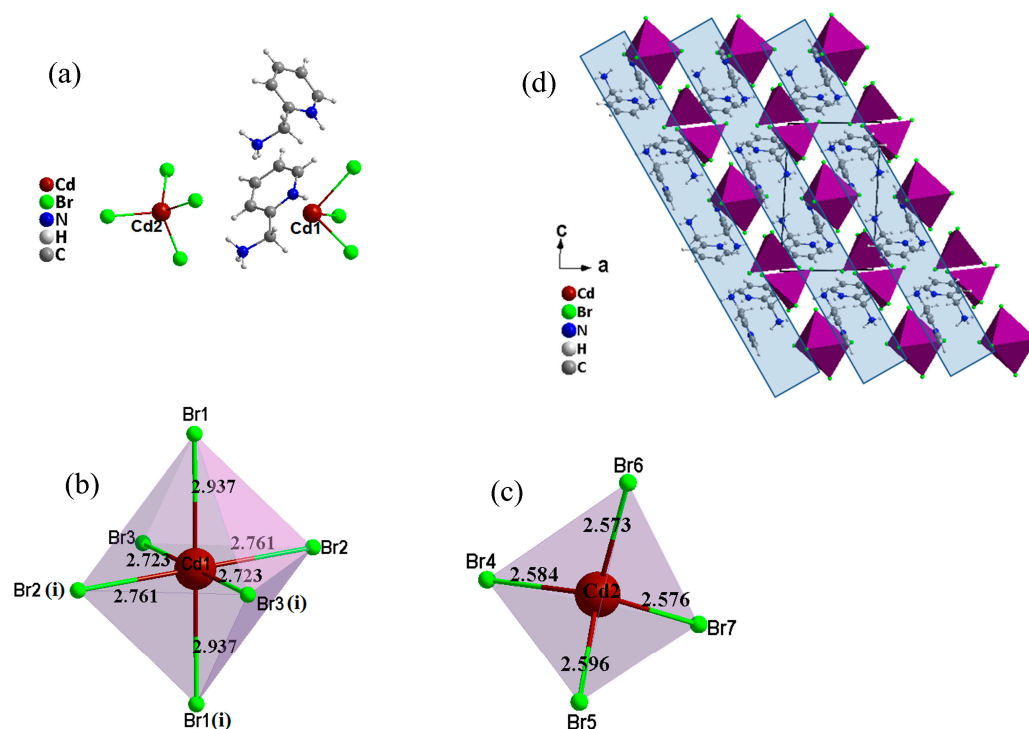


Figure 1. Asymmetric unit of 1 (a), geometric description of the $CdBr_6$ octahedron (b), (symmetry code for generating equivalent atoms: (i) $-x + 1, -y + 2, -z + 1$), geometric description of the $CdBr_4$ tetrahedron (c) and projection of the crystal structure of $(C_6H_{10}N_2)_4[CdBr_6][CdBr_4]_2$ in the (a,c) plane (d).

As illustrated in Figure 1b, the equatorial Cd1–Br bond distances are in the range of 2.7230(5)–2.7611 (5) Å, whereas the axial Cd1–Br bonds extend to 2.9370(5) and 3.0570 (5) Å. The cis angles around the Cd1-center range from 85.655 (15) to 94.346 (15)°, while the trans angles are equal to 180°. We introduce the distortion index (Δ) to quantify the structural distortion within the $CdBr_6$ octahedron given by the following formula:

$$\Delta = \frac{1}{6} \sum_{i=1}^6 \left[\frac{d_i - \bar{d}}{\bar{d}} \right]^2$$

in which \bar{d} is the average Cd–Br bond length, and d_i are the distances of the six individual Cd–Br bonds. The herein obtained Δ value of 1.5×10^{-3} describes the environment around the metal ion to be a slightly distorted octahedron.

Four bromide ions (Br4, Br5, Br6, Br7) ligate the second cadmium center, Cd2, to construct a tetrahedral geometry (Figure 1c). The Cd2–Br bond distances span from 2.5727 (7) to 2.5961 (7) Å and Br–Cd2–Br angles range from 105.84 (2) to 115.98 (2)°.

To precisely describe the coordination polyhedron around the Cd²⁺ cation, we applied the τ_4 parameter, calculated using Equation (1), which is a geometric parameter allowing for the recognition of the geometry around the central atom whether it is square planar geometry or tetrahedral

$$\tau_4 = \frac{[360 - (\alpha + \beta)]}{141} \quad (1)$$

where α and β are the two largest ligand–metal–ligand angles of the coordination sphere. For a perfect square planar geometry, τ_4 is equal to zero, while it becomes unity for ideal tetrahedral geometry. The obtained τ_4 value of 0.94 describes the geometry around the Cd²⁺ to be a quasi-regular tetrahedron.

Figure 1d depicts the arrangement of the various molecular components. The projection along the [010]-direction reveals a layered structure made of an alternate stacking of organic and inorganic layers. It is clear from this figure that the anionic polyhedra forms inorganic layers occupying the (101) planes family between which are embedded the organic layers. Adjacent layers are fastened together through N–H...Br and C–H...Br hydrogen bonds. The geometric parameters of the hydrogen bonds are given in Table 2.

Table 2. Hydrogen bond geometry (Å, °).

D–H...A	D–H	H...A	D...A	D–H...A
N1—H3N1...Br3 ^a	0.91	2.78	3.426(4)	129
N1—H3N1...Br2 ^b	0.91	2.89	3.358(4)	113
N1—H1N1...Br1 ^a	0.91	2.55	3.348(4)	146
N1—H2N1...Br3 ^b	0.91	2.54	3.422(5)	163
N2—HN2...Br1	0.88	2.37	3.241(4)	171
N3—H3N3...Br4 ^c	0.91	2.84	3.546(5)	135
N3—H3N3...Br6 ^d	0.91	2.86	3.462(5)	125
N3—H2N3...Br5	0.91	2.50	3.402(5)	172
N3—H1N3...Br6 ^a	0.91	2.67	3.509(5)	153
N4—Hn4...Br2 ^b	0.88	2.41	3.277(5)	169
C6—H6...Br7 ^e	0.95	2.77	3.568(6)	142
C11—H10...Br1	0.99	2.77	3.452(7)	127
C12—H12...Br7 ^f	0.95	2.80	3.640(7)	148
Symmetry codes: a = −1 + x, y, z; b = 1 − x, −y, 1 − z; c = 1 − x, 1 − y, −z; d = x, −1 + y, z; e = 2 − x, 1 − y, −z; f = 1 − x, 1 − y, 1 − z				

3.2. Infrared Spectroscopy

To confirm the existence of the organic molecules within the structure, FTIR spectroscopy was performed (Figure 2). The band assignments were made by comparison with some previous experimental results reported in the literature for similar compounds [38,39].

The presence of the 2-ammoniummethyl pyridinium ion was confirmed by the deformation and elongation vibrations modes of the NH₃ group appearing around 1614 and 3005 cm^{−1} on each IR spectrum. They are assigned, respectively, to the deformation and elongation vibrations of the NH₃⁺ group. The band observed at 3075 cm^{−1} corresponds to the pyridinium N – H stretching mode ($\nu(\text{NH})$) vibrations. The scissoring (δ) of CH₂ can be found at 1478 cm^{−1}, while the twisting modes related to (CH) groups appear at 775 and 456 cm^{−1}. Two bands situated at 937 and 1234 cm^{−1} are attributed to $\nu(\text{C-N})$ and $\nu(\text{C-C})$, respectively, and the band detected at 625 cm^{−1} was assigned to $\delta(\text{C-C-N})$.

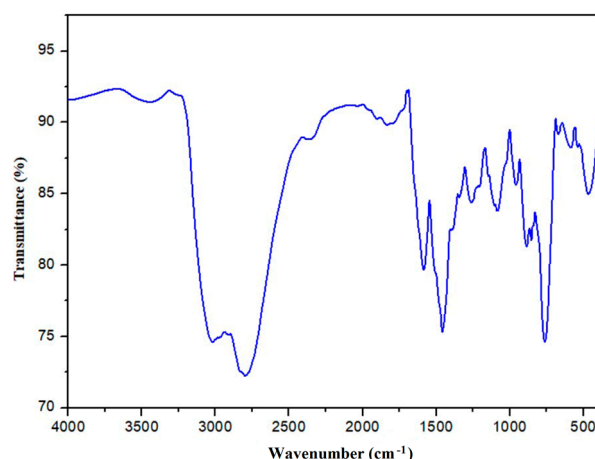


Figure 2. IR spectra of $(\text{C}_6\text{H}_{10}\text{N}_2)_4[\text{CdBr}_6][\text{CdBr}_4]_2$.

3.3. Thermal Analysis

As one can see from the TGA curve (Figure 3), the decomposition of $(\text{C}_6\text{H}_{10}\text{N}_2)_4[\text{CdBr}_6][\text{CdBr}_4]_2$ occurs in two steps. The compound was stable until 200 °C. The first decomposition was detected in the temperature range of 208–333 °C with a weight loss of 40 % and corresponds to the elimination of the organic ammonium salt $(\text{C}_6\text{H}_{10}\text{N}_2)^+ \cdot 2\text{Br}^-$ (Theo: 39.85%). The second decomposition step occurs between 483 and 743 °C and corresponds mainly to the departure of the inorganic part as Br_2 and CdBr_2 gas (Exp: 57% and Theo: 56.8%). The final product, CdO , is presumed to be the remainder compound of the last step (Exp: 3 %; Theo: 2.96%).

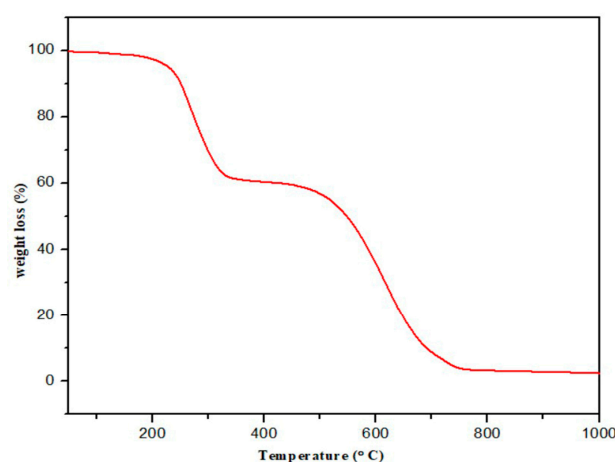


Figure 3. TGA of $(\text{C}_6\text{H}_{10}\text{N}_2)_4[\text{CdBr}_6][\text{CdBr}_4]_2$.

3.4. Optical Analysis

3.4.1. UV–Vis Absorption Properties and Fundamental Gap Energy

To study the optical behavior of $(\text{C}_6\text{H}_{10}\text{N}_2)_4[\text{CdBr}_6][\text{CdBr}_4]_2$, the recorded reflectance data were transformed into absorption mode using the Kubelka–Munk relation (Equation (2)) [40]

$$F(R) = \frac{(1 - R)^2}{2R} = \frac{K}{S} \propto 2\alpha \quad (2)$$

where R denotes the sample reflectance, K is the Kubelka–Munk absorption coefficient, and S is the scattering coefficient.

Similarly to the known Cd-based organic inorganic hybrid materials [18,28,29,34,41], the absorption spectrum presented in Figure 4 shows an intense band in the UV region (at around 225 nm) with three weak bands in the range of 280–550 nm. The band observed at

225 nm is assigned to the intramolecular electronic transfer within the organic cation (π - π^*), while the weak bands result from excitonic transitions within the $[\text{CdBr}_4]^{2-}$ and $[\text{CdBr}_6]^{4-}$ inorganic polyhedra and/or ligand to metal charge transfer from the bromide ions to the Cd cations [33,41]. It can be clearly observed that there is no characteristic absorption band in the region between 400 and 800 nm, which reveals that our synthesized crystal could be exploited for different optical applications such as luminescent devices and lasers. The fundamental band gap and linear absorption coefficient of the material are related through the Tauc function [42]:

$$(\mathbf{F}(\mathbf{R}) \times \mathbf{h}\mathbf{v})^{\frac{1}{m}} = \mathbf{A}_2(\mathbf{h}\mathbf{v} - \mathbf{E}_g) \quad (3)$$

where A_2 and h are a constant and Planck's constant, respectively; m is equal to $1/2$ for a direct allowed transition type and 2 for an indirect allowed transition. According to the Tauc equation, the experimental gap value is obtained from the intercept of the linear portion of the curve $(\mathbf{F}(\mathbf{R})\mathbf{h}\mathbf{v})^{1/m}$ versus the energy (Figure 5). The direct gap value E_g^d was calculated to be 4.97 eV (250 nm), while the indirect gap E_g^i was found to be 4.66 eV, which is close to the gap of the two similar ones in one hybrid compound $[\text{C}_5\text{H}_9\text{-NH}_3]_4\text{CdBr}_6$ (4.58 eV) [30].

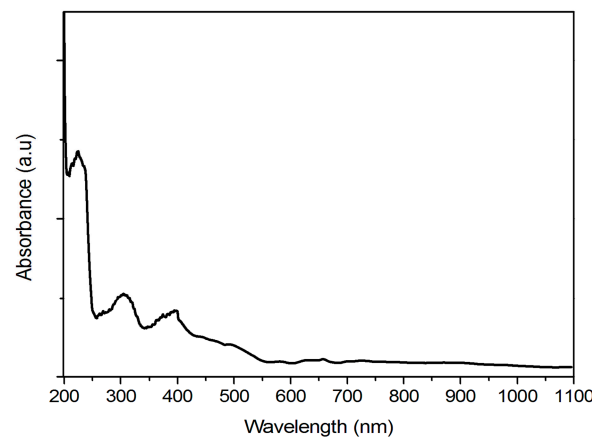


Figure 4. K-M absorption spectrum of $(\text{C}_6\text{H}_{10}\text{N}_2)_4[\text{CdBr}_6][\text{CdBr}_4]_2$.

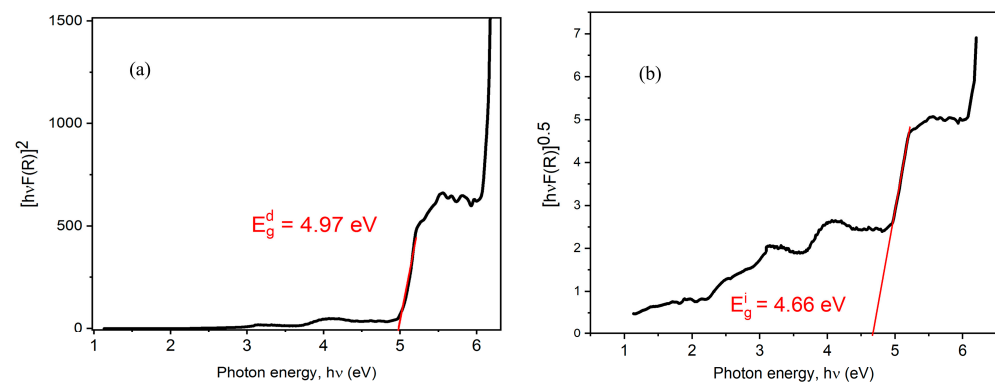


Figure 5. Tauc plot for (a) direct and (b) indirect gap calculation.

3.4.2. Photoluminescence Properties: White Light Emission

In this section, the photoluminescence response of our synthesized material was studied at room temperature as a solid thin film. To scrutinize the luminescence behavior of $(\text{C}_6\text{H}_{10}\text{N}_2)_4[\text{CdBr}_6][\text{CdBr}_4]_2$, the sample was excited using sub-gap photon energy. Figure 6 presents the PL spectrum recorded under 3.3 eV ($\lambda_{\text{Exc}} = 375$ nm) illumination along with a digital photo of the emitted light. As can be seen, under sub-gap excitation, a large emission covering the whole visible region is observed with a broad band centered at about 472 nm with a shoulder around 518 nm and a second peak at 618 nm.

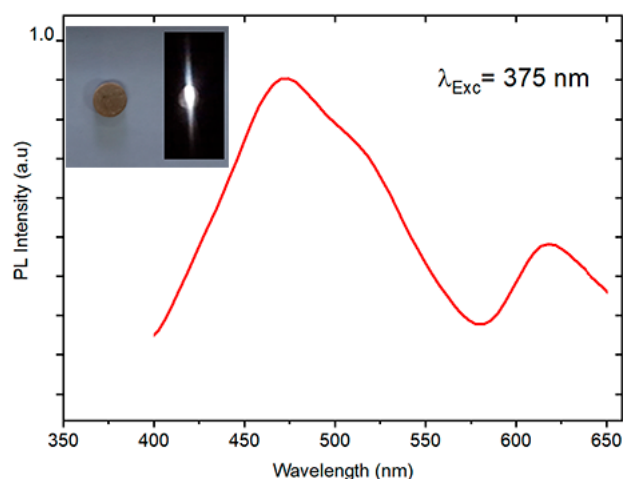


Figure 6. Emission spectrum for $(\text{C}_6\text{H}_{10}\text{N}_2)_4[\text{CdBr}_6][\text{CdBr}_4]_2$ excited at 375 nm (inset: digital photo of the compound before and during excitation).

The time-resolved PL decay was collected at 450 nm at $\lambda_{\text{exc}} = 375$ nm at room temperature. As shown in Figure 7, the lifetime was calculated using the exponential decay fitting to be 1.18 ns. The fast decay of the emission reveals the fluorescence nature of the emitted light. Moreover, the photoluminescence quantum yield of the solid sample was measured to be 1.63 % under 375 nm excitation.

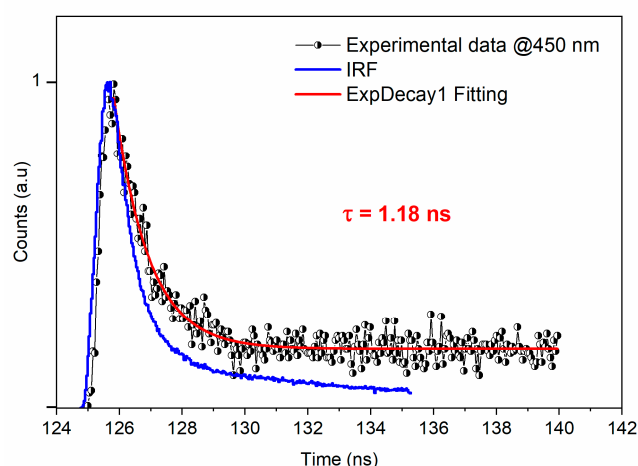


Figure 7. PL lifetime profile of $(\text{C}_6\text{H}_{10}\text{N}_2)_4[\text{CdBr}_6][\text{CdBr}_4]_2$ at $\lambda_{\text{exc}} = 375$ nm.

The visualization of the chromaticity coordinates CIE of the emitted lights under $\lambda_{\text{exc}} = 375$ nm excitation in the chromaticity diagram 1931 (Figure 8) confirms the white light emission from $(\text{C}_6\text{H}_{10}\text{N}_2)_4[\text{CdBr}_6][\text{CdBr}_4]_2$.

For white-light-emitting materials, the color rendering index (CRI) is a prominent parameter that reflects the ability of an illumination source to render the colors of objects compared with daylight [43,44]. The ideal daylight is characterized with chromaticity coordinates of (0.33, 0.33), a correlated color temperature (CCT) of 5500 K and a color rendering index (CRI) of 100. An illumination source with a CRI above 70 is considered satisfactory for interior applications, while that above 80 would be considered good and that above 90 would be considered excellent [43]. A white-light-emitting source with a CRI around 80 is adequate for the human eye, and that with a CRI above 90 is suitable for high-level applications such as photography and surgery [44]. The calculated chromaticity coordinates (x,y), the CCT and the CRI of lights observed under $\lambda_{\text{exc}} = 375$ nm excitation are (0.27, 0.31), 9308 K and 89, respectively. Thus, our material is characterized by cold white light emission and could be used for illumination sources.

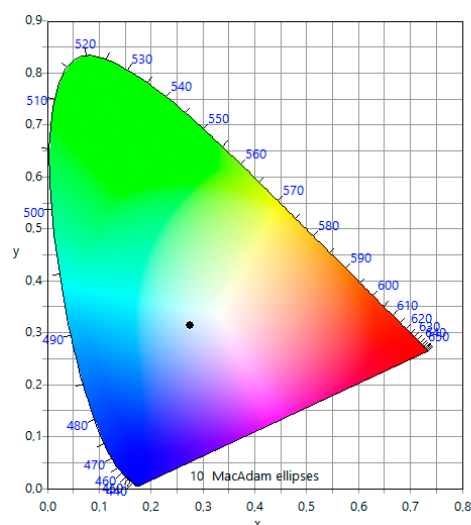


Figure 8. Color coordinates of the emitted white light in the CIE diagram (1931); $\lambda_{\text{exc}} = 375$ nm.

3.4.3. Theoretical Modeling

To gain insight into the optical properties of the $(\text{C}_6\text{H}_{10}\text{N}_2)_4[\text{CdBr}_6][\text{CdBr}_4]_2$, we carried out DFT simulations. All calculations have been carried out using the Quantum Espresso program package [45]. Starting from the crystallographic data, we relaxed the geometry and we simulated the DOS reported in Figure 9. To simulate the electronic structure, we used the HSE06 functional [46] including a 43% Hartree–Fock exchange, a $2 \times 1 \times 1$ k point mesh grid and a cutoff on the wavefunctions of 70 Ryd (280 Ryd on the charge density). For the hybrid HSE06 calculation, we adopted scalar-relativistic norm-conserving pseudo potentials with electrons from H 1s; C 2s2p; N 2s2p; Br 4s4p; Cd 4s4p4d5s shells were explicitly included in calculations. As we can see from the PDOS, the main contribution of the valence band (VB) is mainly associated with the Br, while the conduction states are made up of three bands: the first is only associated with the organic cation contribution, the second is mainly from the organic cation with a slight Cd contribution, and the third one shows the Cd and Br states. This electronic structure suggests an important role of the organic molecule in both absorption and emission processes. In fact, the transition would be expected to be from halogen to organic states, while the emission could proceed in the reverse direction. Another interesting aspect that we can see from the DOS is that the electronic coupling between the organic and inorganic moieties at the VB and CB is very low. Interestingly, we calculated a HOMO/LUMO band gap of 4.1 eV which is lower than the experimental one. However, since the nature of the edge of the VB is mainly localized on the inorganic moiety, the edge CB is mainly composed by the organic states and no coupling between organic and inorganic contribution is found; the lowest VB-CB transition could show a low oscillator strength and does not have significant intensity in absorption, see the green arrow in Figure 9. On the other hand, the transition involving the VB and the second and third CB band around 5 eV would be allowed due to the consistent coupling between the inorganic and organic contribution of the non-occupied states, see the red arrow in Figure 9.

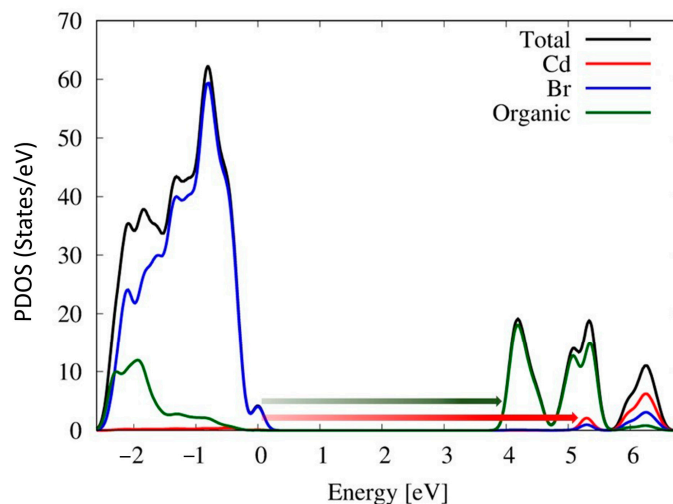


Figure 9. DOS of the $(\text{C}_6\text{H}_{10}\text{N}_2)_4[\text{CdBr}_6][\text{CdBr}_4]_2$. The separated PDOS contributions for each species are reported in different colors.

4. Conclusions

In summation, a new white-light-emitting hybrid material, $(\text{C}_6\text{H}_{10}\text{N}_2)_4[\text{CdBr}_6][\text{CdBr}_4]_2$, containing four- and hexa-coordinated Cd(II) cations was prepared by the slow evaporation method. From XRD data, it is observed that the grown crystal belongs to the triclinic crystal class and centrosymmetric space group $\text{P}\bar{1}$. IR spectroscopy was used to ascertain the assignments of the experimentally observed features. The thermal analysis demonstrates the stability of the synthesized compound up to 200 °C. The optical band gap energy (E_g) of the studied compound was determined by UV–Vis–NIR absorbance measurements and was found to be 4.97 eV for the direct-type one. The solid-state photoluminescence measurements show that the obtained material exhibits cold white light emission under excitation at $\lambda_{\text{exc}} = 375$ nm with a high color rendering index (CRI) of 89, which makes the compound adequate for solid-state lighting sources. Theoretical investigation of the electronic structure shows a good agreement between the calculated and the experimental results and confirms the important role of the organic molecules in the emission mechanism. The fast emission, with a lifetime of 1.18 ns, demonstrates the organic fluorescent nature of this material.

Supplementary Materials: Crystalline data from this new Cd-based hybrid material were deposited at the Cambridge Crystallographic Data Center as Supplementary Publications (CCDC-2278443). Data can be obtained for free at <http://www.ccdc.cam.ac.uk/conts/retrieving.html> (accessed on 18 March 2024) or from Cambridge Crystallographic Data Center, 12 Union Road, Cambridge CB2 1EZ, United Kingdom; fax: +44 1223 336 033; Email: deposit@ccdc.cam.ac.uk.

Author Contributions: Conceptualization, H.N. and R.M.; methodology, I.S., R.M. and H.N.; software, E.M.; validation, A.G., E.M. and N.B.H.; formal analysis, I.S. and R.M.; investigation, A.G. and A.H.; writing—original draft preparation, I.S. and R.M.; writing—review and editing, R.M., E.M. and H.N.; supervision, H.N.; project administration, N.B.H.; funding acquisition, N.B.H. and A.H. All authors have read and agreed to the published version of the manuscript.

Funding: This research received no external funding.

Data Availability Statement: The original data presented in the study are openly available.

Acknowledgments: This work was supported and funded by the Deanship of Scientific Research at Imam Mohammad Ibn Saud Islamic University (IMSIU) (grant number IMSIU-RP23011).

Conflicts of Interest: The authors declare no conflicts of interest.

References

1. Wang, M.S.; Guo, S.P.; Li, Y.; Cai, L.Z.; Zou, J.P.; Xu, G.; Zhou, W.W.; Zheng, F.K.; Guo, G.C. A Direct White-Light-Emitting Metal-Organic Framework with Tunable Yellow-to-White Photoluminescence by Variation of Excitation Light. *J. Am. Chem. Soc.* **2009**, *131*, 13572–13573. [[CrossRef](#)] [[PubMed](#)]
2. Sanchez, C.; Lebeau, B.; Chaput, F.; Boilot, J. Optical Properties of Functional Hybrid Organic-Inorganic Nanocomposites. *Adv. Mater.* **2004**, *15*, 1969–1994. [[CrossRef](#)]
3. Jin, J.-C.; Lin, Y.-P.; Chen, D.-Y.; Lin, B.-Y.; Zhuang, T.-H.; Ma, W.; Gong, L.-K.; Du, K.-Z.; Jiang, J.; Huang, X.-Y. X-Ray Scintillation and Photoluminescence of Isomorphous Ionic Bismuth Halides with [Amim]⁺ or [Ammim]⁺ Cations. *Inorg. Chem. Front.* **2021**, *8*, 4474–4481. [[CrossRef](#)]
4. Borysova, K.V.; Sorg, J.R.; Mikhalyova, E.A.; Oberst, K.; Würtele, C.; Müller-Buschbaum, K. Bismuth Trihalide Based Coordination Polymers with the N- Donor Cyanopyridine as Source for Charge Transfer Based Luminescence. *J. Inorg. Gen. Chem.* **2023**, *649*, e202300131. [[CrossRef](#)]
5. Jin, J.-C.; Lin, Y.-P.; Lin, L.-F.; Xiao, C.; Song, Y.; Shen, N.-N.; Gong, L.-K.; Zhang, Z.-Z.; Du, K.-Z.; Huang, X.-Y. 2,2'-Bipyridyl-1,1'-Dioxide Based Bismuth(III) Bromide Hybrids: Studies on Crystal Structure and Luminescence. *CrystEngComm* **2021**, *23*, 3744–3752. [[CrossRef](#)]
6. Zhuang, T.H.; Lin, Y.M.; Lin, H.W.; Guo, Y.L.; Li, Z.W.; Du, K.Z.; Wang, Z.P.; Huang, X.Y. Luminescence Enhancement and Temperature Sensing Properties of Hybrid Bismuth Halides Achieved via Tuning Organic Cations. *Molecules* **2023**, *28*, 2380. [[CrossRef](#)] [[PubMed](#)]
7. Tang, X.-N.; Gao, C.-C.; Guo, J.-S.; Yuan, M.-Y.; Fan, S.-H.; Li, C.; Liu, G.-N. Crystal Structure and Thermophosphorochromic Property of One-Dimensional Hybrid Haloplumbates with Alkylated Benzothiazole Counter Cations. *Cryst. Growth Des.* **2023**, *23*, 7982–7991. [[CrossRef](#)]
8. Adonin, S.A.; Rakhmanova, M.E.; Samsonenko, D.G.; Sokolov, M.N.; Fedin, V.P. Bi(III) Halide Complexes Containing 4,4'-Vinylenedipyridinium Cation: Synthesis, Structure and Luminescence in Solid State. *Polyhedron* **2015**, *98*, 1–4. [[CrossRef](#)]
9. Li, X.; Wang, Y.; Zhang, Z.; Cai, S.; An, Z.; Huang, W. Recent Advances in Room-Temperature Phosphorescence Metal-Organic Hybrids: Structures, Properties, and Applications. *Adv. Mater.* **2024**, *36*, e2308290. [[CrossRef](#)]
10. Chen, K.; Lai, Y.-C.; Lin, B.C.; Lin, C.C.; Chiu, S.H.; Tu, Z.-Y.; Shih, M.; Yu, P.; Lee, P.-T.; Li, X.; et al. Efficient Hybrid White Light-Emitting Diodes by Organic-Inorganic Materials at Different CCT from 3000K to 9000K. *Opt. Express* **2015**, *23*, A204–A210. [[CrossRef](#)]
11. Bai, T.; Wang, X.; Wang, Z.; Ji, S.; Meng, X.; Wang, Q.; Zhang, R.; Han, P.; Han, K.-L.; Chen, J.; et al. Highly Luminescent One-Dimensional Organic-Inorganic Hybrid Double-Perovskite-Inspired Materials for Single-Component Warm White-Light-Emitting Diodes. *Angew. Chem. Int. Ed. Engl.* **2023**, *62*, e202213240. [[CrossRef](#)] [[PubMed](#)]
12. Cheng, X.; Yue, S.; Chen, R.; Yin, J.; Cui, B.-B. White Light-Emitting Diodes Based on One-Dimensional Organic-Inorganic Hybrid Metal Chloride with Dual Emission. *Inorg. Chem.* **2022**, *61*, 15475–15483. [[CrossRef](#)] [[PubMed](#)]
13. Cho, H.; Jeong, S.H.; Park, M.H.; Kim, Y.H.; Wolf, C.; Lee, C.L.; Heo, J.H.; Sadhanala, A.; Myoung, N.S.; Yoo, S.; et al. Overcoming the Electroluminescence Efficiency Limitations of Perovskite Light-Emitting Diodes. *Science* **2015**, *350*, 1222–1225. [[CrossRef](#)] [[PubMed](#)]
14. Jeong, S.H.; Park, J.; Han, T.H.; Zhang, F.; Zhu, K.; Kim, J.S.; Park, M.H.; Reese, M.O.; Yoo, S.; Lee, T.W. Characterizing the Efficiency of Perovskite Solar Cells and Light-Emitting Diodes. *Joule* **2020**, *4*, 1206–1235. [[CrossRef](#)]
15. Jüstel, T.; Nikol, H.; Ronda, C. New Developments in the Field of Luminescent Materials for Lighting and Displays. *Angew. Chemie Int. Ed.* **1998**, *37*, 3084–3103. [[CrossRef](#)]
16. Pan, X.; Liu, H.; Huynh, U.; Vardeny, Z.V. Magneto-Electroluminescence Response in 2D and 3D Hybrid Organic–Inorganic Perovskite Light Emitting Diodes Magneto-Electroluminescence Response in 2D and 3D Hybrid Organic–Inorganic Perovskite Light Emitting Diodes. *J. Chem. Phys.* **2020**, *152*, 44714. [[CrossRef](#)] [[PubMed](#)]
17. Feng, S.; Huang, Q.; Yang, S.; Lin, Z.; Ling, Q. A Metal-Free 2D Layered Organic Ammonium Halide Framework Realizing Full-Color Persistent Room-Temperature Phosphorescence. *Chem. Sci.* **2021**, *12*, 14451–14458. [[CrossRef](#)] [[PubMed](#)]
18. Msalmi, R.; Elleuch, S.; Hamdi, B.; Zouari, R.; Naili, H. Synthesis, DFT Calculations, Intermolecular Interactions and Third Order Nonlinear Optical Properties of New Organoammonium Tetrabromocadmate (II): (C₅H₆N₂Cl)₂[CdBr₄]·H₂O. *J. Mol. Struct.* **2020**, *1222*, 128853. [[CrossRef](#)]
19. Liu, W.; Lustig, W.P.; Li, J. Luminescent Inorganic–Organic Hybrid Semiconductor Materials for Energy-Saving Lighting Applications. *EnergyChem* **2019**, *1*, 100008. [[CrossRef](#)]
20. Vargas, B.; Coutiño-Gonzalez, E.; Ovalle-Encinia, O.; Sánchez-Aké, C.; Solis-Ibarra, D. Efficient Emission in Halide Layered Double Perovskites: The Role of Sb³⁺ Substitution in Cs₄Cd_{1-x}Mn_xBi₂Cl₁₂ Phosphors. *J. Phys. Chem. Lett.* **2020**, *24*, 10362–10367. [[CrossRef](#)]
21. Bu, Q.; Wang, G.E.; Xu, G.; Long, X.; Xia, Y. Luminescent Inorganic–Organic Hybrid with Tunable Red Light Emissions by Neutral Molecule Modification. *Inorg. Chem. Commun.* **2020**, *116*, 107909. [[CrossRef](#)]
22. Uchida, Y. Lighting Theory and Luminous Characteristics of White Light-Emitting Diodes. *Opt. Eng.* **2005**, *44*, 124003. [[CrossRef](#)]
23. Taguchi, T. Present Status of White LED Lighting Technologies in Japan. *J. Light Vis. Environ.* **2003**, *27*, 131–139. [[CrossRef](#)]

24. Temerova, D.; Chou, T.C.; Kisel, K.S.; Eskelinen, T.; Kinnunen, N.; Jänis, J.; Karttunen, A.J.; Chou, P.T.; Koshevoy, I.O. Hybrid Inorganic–Organic Complexes of Zn, Cd, and Pb with a Cationic Phenanthro–Diimine Ligand. *Inorg. Chem.* **2022**, *61*, 19220–19231. [[CrossRef](#)] [[PubMed](#)]
25. Sun, C.; He, W.-L.; Liu, M.-J.; Pan, W.-J.; Dong, L.-F.; Chen, G.; Liu, G.-D.; Lei, X.-W. Zero-Dimensional Hybrid Cd-Based Perovskites with Broadband Bluish White-Light Emissions. *Chem. Asian J.* **2020**, *15*, 3050–3058. [[CrossRef](#)] [[PubMed](#)]
26. Qi, Z.; Chen, Y.; Guo, Y.; Yang, X.; Zhang, F.Q.; Zhou, G.; Zhang, X.M. Broadband White-Light Emission in a One-Dimensional Organic–Inorganic Hybrid Cadmium Chloride with Face-Sharing CdCl₆octahedral Chains. *J. Mater. Chem. C* **2021**, *9*, 88–94. [[CrossRef](#)]
27. Wang, J.; Liu, Y.; Han, S.; Li, Y.; Xu, Z.; Luo, J.; Hong, M.; Sun, Z.; Liu, Y.; Han, S.; et al. Ultrasensitive Polarized-Light Photodetectors Based on 2D Hybrid. *Sci. Bull.* **2020**, *66*, 158–163. [[CrossRef](#)]
28. Jellali, H.; Msalmi, R.; Smaoui, H.; Elleuch, S.; Tozri, A.; Roisnel, T.; Mosconi, E.; Althubiti, N.A.; Naili, H. Zn²⁺ and Cu²⁺ Doping of One-Dimensional Lead-Free Hybrid Perovskite ABX₃ for White Light Emission and Green Solar Cell Applications. *Mater. Res. Bull.* **2022**, *151*, 111819. [[CrossRef](#)]
29. Msalmi, R.; Elleuch, S.; Hamdi, B.; Abd El-Fattah, W.; Ben Hamadi, N.; Naili, H. Organically Tuned White-Light Emission from Two Zero-Dimensional Cd-Based Hybrids. *RSC Adv.* **2022**, *12*, 10431. [[CrossRef](#)]
30. Sasa, W.; Li, L.; Sun, Z.; Ji, C.; Liu, S.; Wu, Z.; Zhao, S.; Hong, M.; Luo, J. A Semi-Conductive Organic–Inorganic Hybrid Emits Pure White Light with Ultrahigh Color Rendering Index. *J. Mater. Chem. C* **2017**, *5*, 4731–4735. [[CrossRef](#)]
31. Gassara, M.; Msalmi, R.; Liu, X.; Hassen, F.; Moliterni, A.; Ben Hamadi, N.; Guesmi, A.; Khezami, L.; Soltani, T.; Naili, H. A Promising 1D Cd-Based Hybrid Perovskite-Type for White-Light Emission with High-Color-Rendering Index. *RSC Adv.* **2022**, *12*, 33516–33524. [[CrossRef](#)] [[PubMed](#)]
32. Ohnishi, A.; Yamada, T.; Yoshinari, T.; Akimoto, I.; Kanno, K.; Kamikawa, T. Emission Spectra and Decay Characteristics in Photo-Stimulated (C_nH_{2n+1}NH₂)₂CdCh: N = 1, 2, 3. *J. Electron Spectros. Relat. Phenomena* **1996**, *79*, 163–166. [[CrossRef](#)]
33. Rocanova, R.; Ming, W.; Whiteside, V.R.; McGuire, M.A.; Sellers, I.R.; Du, M.H.; Saparov, B. Synthesis, Crystal and Electronic Structures, and Optical Properties of (CH₃NH₃)₂CdX₄ (X = Cl, Br, I). *Inorg. Chem.* **2017**, *56*, 13878–13888. [[CrossRef](#)] [[PubMed](#)]
34. Rocanova, R.; Houck, M.; Yangui, A.; Han, D.; Shi, H.; Wu, Y.; Glatzhofer, D.T.; Powell, D.R.; Chen, S.; Fourati, H.; et al. Broadband Emission in Hybrid Organic–Inorganic Halides of Group 12 Metals. *ACS Omega* **2018**, *3*, 18791–18802. [[CrossRef](#)] [[PubMed](#)]
35. Liu, S.; Fang, X.; Lu, B.; Yan, D. Wide Range Zero-Thermal-Quenching Ultralong Phosphorescence from Zero-Dimensional Metal Halide Hybrids. *Nat. Commun.* **2020**, *11*, 4649. [[CrossRef](#)] [[PubMed](#)]
36. Yao, Z.; Chen, W.; Hu, R. Photoluminescence and Theoretical Study of [∞ 1(Cd₂Cl₆)]₂[(CdCl₄)]₃[(N,N′-Dimethyl- 4,4′-Bipyridinium)]. *Indian J. Chem.* **2015**, *54A*, 489–493.
37. Sheldrick, G.M. Crystal Structure Refinement with SHELXL. *Acta Crystallogr. Sect. C Struct. Chem.* **2015**, *71*, 3–8. [[CrossRef](#)] [[PubMed](#)]
38. Hamdi, I.; Bkhairia, I.; Roodt, A.; Roisnel, T.; Nasri, M.; Naili, H. Synthesis, Intermolecular Interactions and Biological Activities of Two New Organic–Inorganic Hybrids C₆H₁₀N₂2Br and C₆H₁₀N₂2Cl·H₂O. *RSC Adv.* **2020**, *10*, 5864–5873. [[CrossRef](#)] [[PubMed](#)]
39. Hamdi, I.; Mhadhbi, N.; Issaoui, N.; Roodt, A.; Turnbull, M.M.; Naili, H. Design, Synthesis and Physico-Chemical Studies of a Co(II)/Co(III) Mixed-Valence Complex: An Experimental and DFT Approach. *J. Mol. Struct.* **2021**, *1237*, 130384. [[CrossRef](#)]
40. Sun, J.; Wang, H.; Zhang, Y.; Zheng, Y.; Xu, Z.; Liu, R. Structure and Luminescent Properties of Electrodeposited Eu³⁺-Doped CaF₂ Thin Films. *Thin Solid Films* **2014**, *562*, 478–484. [[CrossRef](#)]
41. Msalmi, R.; Dammak, K.; Elleuch, S.; Hamdi, B.; Tozri, A.; Naili, H. Optoelectronic, Luminescence, and Nonlinear Properties of a Non-Centrosymmetric Cd(II)-Based Complex. *J. Phys. Chem. Solids* **2022**, *163*, 110567. [[CrossRef](#)]
42. Zahan, M.; Podder, J. Surface Morphology, Optical Properties and Urbach Tail of Spray Deposited Co₃O₄ Thin Films. *J. Mater. Sci. Mater. Electron.* **2019**, *30*, 4259–4269. [[CrossRef](#)]
43. Ye, S.; Xiao, F.; Pan, Y.X.; Ma, Y.Y.; Zhang, Q.Y. Phosphors in Phosphor-Converted White Light-Emitting Diodes: Recent Advances in Materials, Techniques and Properties. *Mater. Sci. Eng. R Rep.* **2010**, *71*, 1–34. [[CrossRef](#)]
44. Rea, M.S.; Freyssonier, J.P. Color Rendering: Beyond Pride and Prejudice. *Color Res. Appl.* **2010**, *35*, 401–409. [[CrossRef](#)]
45. Giannozzi, P.; Baroni, S.; Bonini, N.; Calandra, M.; Car, R.; Cavazzoni, C.; Ceresoli, D.; Chiarotti, G.L.; Cococcioni, M.; Dabo, I.; et al. Quantum Espresso: A Modular and Open-Source Software Project for Quantum Simulations of Materials. *J. Phys. Condens. Matter* **2009**, *21*, 395502. [[CrossRef](#)]
46. Heyd, J.; Scuseria, G.E.; Ernzerhof, M. Hybrid Functionals Based on a Screened Coulomb Potential. *J. Chem. Phys.* **2003**, *118*, 8207–8215. [[CrossRef](#)]

Disclaimer/Publisher’s Note: The statements, opinions and data contained in all publications are solely those of the individual author(s) and contributor(s) and not of MDPI and/or the editor(s). MDPI and/or the editor(s) disclaim responsibility for any injury to people or property resulting from any ideas, methods, instructions or products referred to in the content.